4. Ozone and Water Vapor

J. HARRIS (EDITOR), J. BARNES, G. CARBAUGH, D. CHAO, M. CLARK, R. EVANS, E. HALL, B. JOHNSON, A. JORDAN, M. O'NEILL, S. OLTMANS, D. QUINCY, D. SHERMAN, H. VÖMEL, AND B. WALSH

4.1. CONTINUING PROGRAMS

4.1.1. TOTAL OZONE OBSERVATIONS

Total ozone observations continued throughout 2002 and 2003 at the 16 stations that constitute the U.S. Dobson spectrophotometer network (Table 4.1). Of the 16 stations, CMDL personnel operated five, the National Weather Service (NWS) operated four, National Aeronautics and Space Administration (NASA) operated one, two are university stations, and four are foreign cooperative stations. All instruments in the network are either fully automated or semiautomated, except for the one manual instrument at the Peruvian site. In addition to the instruments in the Dobson network, a Brewer instrument was operated on a nearly continuous basis in Boulder.

Observations at Florida State University, Tallahassee, continue, but they were not made on a regular basis because of personnel problems. Therefore, the data record is not very useful in 2002 or 2003. The observations at Caribou, Maine, became less frequent because of personnel problems as well. Data taken at l'Observatoire de Haute Provence (OHP), France, are suspect from October 2002 to July 2003 due to damage from rain entering the instrument shelter. The instrument was repaired in July 2003 and put back in service in August 2003. The automated systems in Boulder, Colorado, Fairbanks, Alaska, and at OHP were upgraded with more modern data acquisition and control electronics.

Many of the operational sites transfer data electronically once a day allowing for access to preliminary ozone data in near real time. All data submitted to CMDL were processed on a monthly basis and then archived at the World Ozone and Ultraviolet Data Centre (WOUDC), Canada, in *Ozone Data for the World* (http://www.woudc.org). Table 4.2 lists the monthly mean total ozone amounts measured at the stations in the network for 2002 and 2003.

Observations of total ozone at the South Pole Observatory (SPO) using the Dobson spectrophotometer are limited to sunlit or moonlit periods. In the winter months only a few moon observations can be made, and during twilight periods no Dobson observations are available. By using the integrated column ozone amount from the ozonesonde vertical profile measurement, a more complete record of total ozone observations was compiled. Using the statistical model from the work of *Harris et al*. [2001] the long-term changes were described (Figure 4.1a). The decline in column ozone began in the 1970s and was less precipitous in the 1990s. The overall growth rate (decline) was $-6.5 \pm 0.5\%$ per decade. The growth rate in the most recent years suggests that declines may be leveling off. Signs of ozone recovery at SPO are several years away, however, because near maximum ozone destruction potential at SPO will continue to exist until ozone destroying halogens are reduced further in the stratosphere.

At midlatitudes in the Northern Hemisphere, total ozone observations at several sites in the United States approach 40 years in length. At these sites column ozone also began a small decline in the 1970s with more pronounced decreases in the 1980s (Figure 4.1b). In recent years there was a flattening of the tendency (trend) curves. This may represent the influence of declining halogens, but this is not unambiguous at this time. Also, at the Mauna Loa Observatory (MLO) and the American Samoa Observatory (SMO) there have been significant declines in the 1970s and 1980s (Figure 4.1c). However, the decline has not continued in recent years.

Table 4.1. Dobson Ozone Spectrophotometer Station Network for 2002-2003

Station	Period of Record	Instrument No.	Agency
Bismarck, North Dakota	1 Jan. 1963-present	33	NOAA
Caribou, Maine	1 Jan. 1963-present	34	NOAA
Wallops Is., Virginia	1 July 1967-present	38	NOAA, NASA
SMO	19 Dec. 1975-present	42	NOAA
Tallahassee, Florida	2 May 1964-30 Nov. 1989; 1 Nov. 1992-present	58	NOAA, Florida State University
Boulder, Colorado	1 Sept. 1966-present	61	NOAA
Fairbanks, Alaska	6 March 1984-present	63	NOAA, University of Alaska
Lauder, New Zealand	29 Jan. 1987-present	72	NOAA, National Institute of Water and Atmospheric Research
MLO	2 Jan. 1964-present	76	NOAA
Nashville, Tennessee	2 Jan. 1963-present	79	NOAA
Perth, Australia	30 July 1984-present	81	NOAA, Australian Bureau Meteorology
SPO	17 Nov. 1961-present	82	NOAA
Haute Provence, France	2 Sept. 1983-present	85	NOAA, Centre National de la Recherche Scientifique, University of Riems
Marcapomacocha, Peru	26 Feb. 2001-present	87	NOAA, Servicio Nacional de Meteorologia e Hidrologia
BRW	6 June 1986-present	91	NOAA
Fresno, California/ Hanford, California	22 June 1983-13 March 1995; 15 March 1995-present	94	NOAA

Table 4.2. Provisional 2002 and 2003 Monthly Mean Total Ozone Amounts (DU)

Station	Jan.	Feb.	March	April	May	June	July	Aug.	Sept.	Oct.	Nov.	Dec.
					2002							
Bismarck, North Dakota	339	338	383	360	364	327	302	303	288	303	305	323
Caribou, Maine	—	[368]	[383]	[379]	[372]	[345]	—	—	—	—	—	—
Wallops Is., Virginia	283	308	310	320	329	325	312	307	280	[270]	[282]	298
SMO	257	253	247	246	240	248	242	246	261	251	249	250
Tallahassee, Florida	#	#	#	#	#	#	#	#	#	#	#	#
Boulder, Colorado	304	307	320	306	338	315	297	297	286	286	296	320
Fairbanks, Alaska	—	[396]	385	412	[388]	[323]	330	313	304	294	[284]	—
Lauder, New Zealand	272	272	264	267	290	299	335	372	376	350	320	296
MLO	228	232	243	262	267	270	265	259	251	251	254	239
Nashville, Tennessee	283	304	301	309	324	328	316	306	279	283	300	303
Perth, Australia	275	266	261	277	266	269	277	293	313	306	301	287
SPO	262	257	[249]	—	[212]	[244]	—	—	—	192	339	305
Haute Provence, France	299	[294]	334	346	337	331	325	314	—	—	—	295
Marcapomacocha, Peru	255	254	257	252	242	242	245	249	255	254	255	251
BRW	—	[349]	388	[440]	357	[352]	324	294	[293]	—	—	—
Hanford, California	292	278	309	320	339	307	296	291	282	285	285	309
					2003							
Bismarck, North Dakota	339	401	385	355	352	342	305	296	300	280	313	320
Caribou, Maine	—	—	—	—	—	[330]	[335]	[311]	286	[319]	[297]	—
Wallops Is., Virginia	[352]	[338]	352	338	[347]	315	305	—	—	—	[264]	294
SMO	242	249	240	244	250	254	250	249	260	255	251	254
Tallahassee, Florida	#	#	#	#	#	#	[306]	#	#	#	#	#
Boulder, Colorado	298	361	354	336	332	314	290	288	283	268	276	294
Fairbanks, Alaska	—	[422]	451	[443]	—	—	[318]	318	—	[328]	—	—
Lauder, New Zealand	277	272	265	272	291	299	336	346	372	368	328	290
MLO	232	251	267	287	285	272	268	267	262	250	241	235
Nashville, Tennessee	317	[324]	345	329	339	329	317	308	297	286	273	291
Perth, Australia	269	267	266	266	262	287	297	313	321	324	307	281
SPO	268	245	—	—	—	—	—	—	—	148	221	274
Haute Provence, France	354	363	344	366	332	321	—	[316]	312	291	[323]	295
Marcapomacocha, Peru	248	251	252	248	249	247	252	252	255	—	—	—
BRW	—	—	457	441	409	343	327	308	[299]	[272]	—	—
Hanford, California	284	331	327	348	324	309	[314]	297	284	268	280	286

Monthly mean ozone values in square brackets are derived from observations made on fewer than 10 days per month.
—, no data; #, data are too sparse for meaningful monthly averages.

4.1.2. UMKEHR OBSERVATIONS

Umkehr observations made with the automated Dobson network instruments continued in 2002 and 2003 at Boulder, Colorado; OHP; Lauder, New Zealand; MLO; Perth, Western Australia; and at the Geophysical Institute, University of Alaska. Data processing was completed for all stations through December 2003 and the vertical profiles are available from WOUDC. Problems at Perth have yet to be completely resolved, but data that passes the current criteria for acceptable inversions were sent to WOUDC with an explanatory paragraph for potential users.

4.1.3. CALIBRATION OF DOBSON SPECTROPHOTOMETERS

Six Dobson ozone spectrophotometers in the CMDL network, as well as eight others, were calibrated during 2002 and 2003. Table 4.3 lists all the instruments calibrated with the resulting calibration difference expressed as a percent ozone difference. This percent difference is the difference between the ozone calculated from the test and from the standard instrument using the measurements based on the most common observation type (A/D wavelength observation on direct sun). The value is then averaged over μ (optical path length through the atmosphere calculated from solar zenith angle) values of 1, 2, and 3 and normalized to a total ozone value of 300 Dobson units (DU). This number represents the instrument measurement status before any repair or calibration adjustment is made. The table also lists the location of the calibration and the standard instrument used. The Boulder station instrument (D061) is normally compared with the primary standard (D083) whenever intercomparisons are made. The MLO station instrument (D076) is compared with the primary standard each summer. The secondary standard (D065) is compared with the primary standard twice yearly. These instruments are maintained to within ±1% of the primary standard. Instrument D065 has maintained calibration to within ±0.5% since 1994.

CMDL participated in international Dobson spectrophotometer calibrations at the Japan Meteorological Agency Aerological Observatory in Tsukuba, Japan; in the Meteoswiss Lichtklimatisches Observatorium (LKO) in Arosa, Switzerland; and in the Argentine Meteorological Service Villa Ortuzar Observatory in 2003 as part of its role as the World Center for Dobson Calibrations. The European regional standard Dobson instrument was calibrated in Boulder during June 2002.

Table 4.3. Dobson Ozone Spectrophotometers Calibrated in 2002-2003

Station	Instrument Number	Original Calibration Date	Calibration Correction (%)	Standard Number	Location
		2002			
Hohenpeissenberg, Germany (European regional Standard)	64	17 July 1999	+0.0	83	Boulder, Colorado
WMO Spare	67	N/A	N/A	83	Boulder, Colorado
WMO Spare	105	N/A	N/A	83	Boulder, Colorado
		2003			
Kunming, China	3	1979	-4.2	116	Tsukuba, Japan
Beijing, China	75	1999	+1.8	116	Tsukuba, Japan
NASA Wallops Island Flight Center	38	7 May1999	-0.7	83	Boulder, Colorado
Florida State University, Tallahassee	58	26August 1998	+3.5	83	Boulder, Colorado
University of Alaska, Fairbanks	63	17 September 1998	-1.0	83	Boulder, Colorado
NWSO Hanford, California	94	February 1997	+0.9	65	Boulder, Colorado
L'Observatoire de Haute Provence, France	85	25 July 1999	0.0	64	Arosa, Switzerland
Havana, Cuba	67	N/A	N/A	65	Buenos Aires, Argentina
Marcapomacocha, Peru	87	7 December 1999	+1.5	65	Buenos Aires, Argentina
Natal, Brazil	93	25 June 1994	+1.6	65	Buenos Aires, Argentina
Buenos Aires, Argentina	97	7 June 1998	-2.0	65	Buenos Aires, Argentina
Marambio, Antarctica	99	1 August 2001	+0.8	65	Buenos Aires, Argentina
Cachoeira Paulista, Brazil	114	7 December 1999	+5.0	65	Buenos Aires, Argentina
Ushuaia, Argentina	131	7 December 1999	+1.8	65	Buenos Aires, Argentina
Comodoro Rivadavia, Argentina	133	27 November 1999	0.0	65	Buenos Aires, Argentina
Salto, Uruguay	134	Calibration broken	N/A	65	Buenos Aires, Argentina

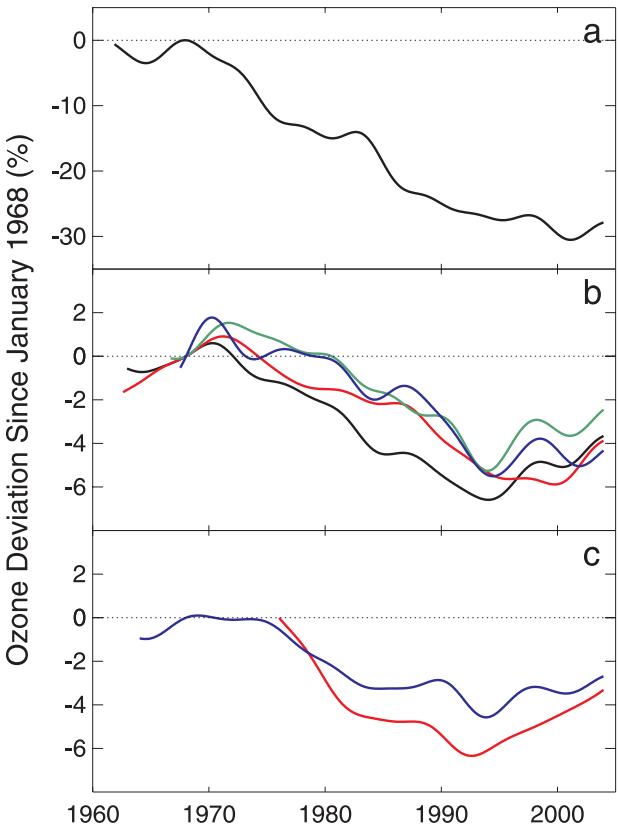

Figure 4.1. Total ozone tendency curves for (a) SPO; (b) midlatitude sites: Bismarck, North Dakota (black); Nashville, Tennessee (red); Boulder, Colorado (green); Wallops Island, Virginia (blue); and (c) SMO (red) and MLO (blue).

Two WMO instruments were renovated in Boulder. Instrument D067 was rebuilt in Boulder and was calibrated in Buenos Aires before going to Havana, Cuba. Instrument D102 was donated to the WMO by the Meteorological Service of Canada and restored to operation in Boulder. NASA is temporarily using the instrument for special optical tests.

4.1.4. Surface Ozone

Observations of surface ozone continued at each of the four baseline observatories as well as Niwot Ridge, Colorado; Westman Islands, Iceland; and Arrival Heights, Antarctica. At Summit Station, Greenland, year-round operations ceased in July 2002. However, operations resumed in July 2003 with the expectation that year-round observations will be made in the future. Data from BRW, MLO, SMO, and SPO were processed through 2003. At Arrival Heights a TEI 49C ozone analyzer was installed in December 2002 and operated in parallel with the Dasibi 1003AH ozone analyzer until the Dasibi was removed at the end of 2003. With the establishment of baseline station operations at Trinidad Head, California, a TEI 49C ozone analyzer was installed in April 2002. After a 5-year gap in measurements in Bermuda, a TEI 49C ozone analyzer was installed in February 2003 at the Tudor Hill, Bermuda, site where previous observations were made. Unfortunately, in September 2003 Hurricane Fabian severely damaged Bermuda and power was not restored to the site by the end of 2003. New TEI 49C analyzers were also installed at BRW; MLO; Westman Islands, Iceland; and Niwot Ridge, Colorado. At BRW and MLO the new analyzers are running in parallel with older analyzers at the station. At SPO the TEI 49C analyzer, in operation since December 1999, was replaced with a new analyzer in November 2002 that operates in parallel with the Dasibi instrument. In addition, a new, high-elevation site was established at Niwot

Ridge (Tundra Laboratory). Also, a new surface ozone measurement program was initiated at Lauder, New Zealand. At Westman Islands and Niwot Ridge data are available only in 2003 after the new analyzers were installed due to instrument and data system problems with the older instruments. Locations, and the period of data record for each of the surface ozone sites, are given in Table 4.4. The monthly mean data for each site are given in Table 4.5 for 2002 and 2003. For MLO the average is based on

Table 4.4. CMDL Surface Ozone Station Locations

Station Name	Code	Latitude	Longitude	Altitude (m)	Observation Record
Summit, Greenland	SU	72.57°N	38.48°W	3238	2000-Present
Barrow, Alaska	BR	71.32°N	156.61°W	8	1973-Present
Storhofdi, Iceland	VM	63.34°N	20.29°W	127	1992-Present
Trinidad Head, California.	TH	41.05°N	124.15°W	107	2002-Present
Niwot Ridge, Colorado C-1	NW	40.04°N	105.54°W	3022	1991-Present
Niwot Ridge Tundra Laboratory	TL	40.05°N	105.59°W	3538	2003-Present
Tudor Hill, Bermuda	BM	32.27°N	64.88°W	30	1988-1998, 2003-Present
Mauna Loa, Hawaii	ML	19.54°N	155.58°W	3397	1973-Present
Ragged Point, Barbados	BA	13.17°N	59.43°W	45	1989-1995
Cape Matatula, Samoa	SM	14.23°S	170.56°W	77	1976-Present
Lauder, New Zealand	LA	45.04°S	169.68°E	370	2003-Present
Arrival Heights, Antarctica	AH	77.80°S	166.78°E	50	1998-Present
South Pole, Antarctica	SP	90.00°S		2837	1975-Present

Table 4.5. Monthly Mean Surface Ozone Mixing Ratios (ppbv)

Year	Jan.	Feb.	March	April	May	June	July	Aug.	Sept.	Oct.	Nov.	Dec.
						Barrow						
2002	32.0	35.1	26.2	16.5	20.4	24.1	20.6	21.7	26.0	31.4	33.3	31.5
2003	32.8	30.7	23.1	22.0	30.0	29.9	22.7	24.4	28.4	32.1	35.4	34.5
						Mauna Loa (10-189 UT, nighttime only)						
2002	42.4	44.9	45.2	50.7	36.9	42.5	37.7	39.6	38.1	46.3	47.1	45.4
2003	44.6	46.7	44.9	44.4	39.6	34.5	35.6	36.3	41.2	41.3	43.8	38.5
						South Pole						
2002	26.5	19.8	19.8	24.3	28.7	31.4	32.3	31.8	32.0	27.5	29.1	32.0
2003	26.7	20.9	24.5	27.4	30.2	32.4	34.0	33.7	33.8	30.1	30.8	31.7
						Samoa						
2002	8.7	5.9	5.9	8.0	12.9	16.3	15.7	20.0	17.9	15.6	11.1	11.7
2003	5.0	7.2	5.9	9.4	14.8	21.3	14.1	15.1	15.6	14.2	10.6	9.2
						Trinidad Head (23-03 UT, afternoon)						
2002	—	—	—	44.4	41.9	31.3	27.6	28.9	31.5	33.5	32.4	36.1
2003	29.3	36.8	42.0	49.6	43.9	40.3	27.0	30.9	35.7	33.0	34.7	34.2
						Niwot Ridge (C-1)						
2003	—	—	—	—	—	—	—	—	—	44.6	45.4	44.5
						Niwot Ridge (Tundra Laboratory)						
2003	—	—	—	—	—	—	—	—	—	44.8	48.1	46.6
						Summit						
2002	46.2	44.4	47.9	53.2	57.1	55.2	49.5					
2003	—	—	—	—	—	—	—	45.4	43.4	43.3	42.8	42.9
						Bermuda						
2003	—	—	46.2	46.9	41.6	28.4	19.9	28.3	—	—	—	—
						Arrival Heights						
2000	12.2	14.8	18.2	24.1	28.4	32.0	32.5	31.7	27.7	23.0	20.5	14.2
2001	12.6	16.1	19.8	24.2	27.9	31.7	35.2	34.8	31.3	27.7	20.9	17.1
2002	15.4	17.1	20.1	25.1	27.8	34.2	24.2	35.9	37.3	31.9	29.4	23.9
2003	16.5	18.5	23.3	27.7	31.8	34.5	35.7	34.6	34.1	28.7	25.4	20.5
						Westman Islands						
2003	—	—	—	—	—	—	—	—	34.6	37.1	39.7	40.3

downslope (10-18 Universal Time Coordinated (UTC)) data and at Trinidad Head afternoon (23-03 UTC) averages are reported. Hourly and monthly average data from the beginning of each station record through 2003 are available through the CMDL Web site (www.cmdl.noaa.gov) by clicking on "Data" and then "Surface Ozone."

Trends were computed for each of the four long-term data sets (Figure 4.2) using the method described in the work of *Harris et al.* [2001]. The data are modeled by fitting a seasonal and long-term variation with the trend determined by averaging the monthly instantaneous growth rates (not shown) and using Monte Carlo calculations to determine the uncertainty. The numerical trends are summarized in Table 4.6. At BRW surface ozone amounts were generally increasing in the 1980s and early 1990s with large fluctuations occurring in recent years. At MLO there has been an overall increase, but after relatively higher ozone amounts in the late 1990s the past several years have had lower values. At SMO ozone mixing ratios remained relatively unchanged. The significant decline at SPO seen through the 1980s and early 1990s has nearly recovered in recent years with little overall change now evident.

4.1.5. OZONESONDES

Table 4.7 lists the CMDL ozonesonde sites for 2002-2003. Eight sites launched weekly ozonesondes, while daily ozonesondes were launched for 1 month in the spring of 2002 at Trinidad Head, California, as part of the Intercontinental Transport and Chemical Transformation 2002 (ITCT 2K2) field project. Additional ozonesondes were also launched at SPO from 15 June to 15 October 2003 as part of the Quantitative Understanding of Ozone Losses by Bipolar Investigations (QUOBI) field project at Antarctica.

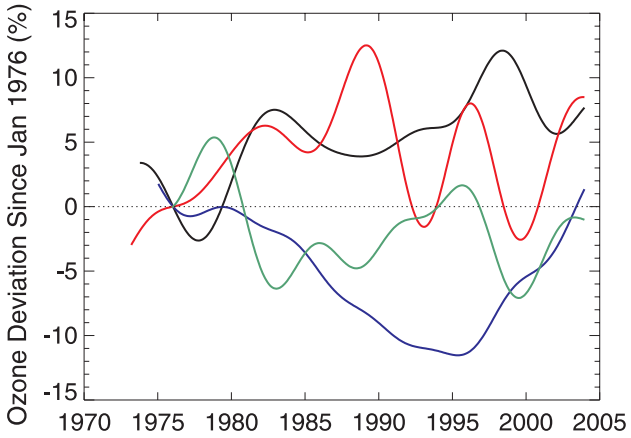

Figure 4.2. Tendency of surface ozone mixing ratios at BRW (red), MLO (black), SMO (green), and SPO (blue). The curves are a smooth fit to the filtered residuals (the difference between the modeled and measured mixing ratios).

Table 4.6. Average Growth Rate and 95% Confidence Interval for Surface Ozone Mixing Ratio at Four CMDL Sites*

	BRW	MLO	SMO	SPO
Trend (C. I.)	3.7 (1.3)	1.1 (1.1)	-0.05 (1.6)	-0.1 (0.6)

*Values in percent per decade.

All of the sites and campaigns used electrochemical concentration cell (ECC) ozonesondes purchased from Environmental Science Corporation (ENSCI) and Science Pump Corporation. The ozonesondes' sensing solution consisted of 3 ml of 2% potassium iodide solution. Data were processed using CMDL average pump efficiencies [*Johnson et. al.*, 2002]. Pump efficiencies are determined in the CMDL environmental chamber by measuring ozonesonde flow rates at ambient pressures between 100 and 5 hPa using an oil bubble flowmeter. About ten new ozonesondes per year are selected randomly for calibration in our environmental chamber to ensure that the average pump efficiency remains consistent.

Ozonesonde performance is judged by comparing total integrated ozone with the Dobson spectrophotometer measurements at CMDL field sites at Boulder, SPO, SMO and MLO. The elevation difference between Hilo, Hawaii (11 m) and MLO (3397 m) is compensated for by adding an average tropospheric amount of 7 DU to the MLO values. Table 4.8 lists the average differences. The residual ozone above the ozonesonde balloon burst was computed by the constant mixing ratio (CMR) method and using the climatological tables from the Solar Backscatter UltraViolet data (SBUV) given by *McPeters et al.* [1997]. The CMR method gives higher residual values than the SBUV, especially at the tropical locations at SMO and Fiji, but gives lower residuals than the SBUV residuals at SPO.

It is common to use the percentage differences in Table 4.8 as a linear correction factor to normalize the ozonesonde profile to the Dobson total column ozone. However, there is some concern that a linear correction may skew profiles incorrectly. Therefore, no Dobson normalization corrections were applied to any of the archived CMDL ozonesonde data. An example of how a linear correction over an entire profile could inadvertently create an error can be observed in some of the reconditioned ozonesondes flown. The Boulder site is the only CMDL location that uses reconditioned ozonesondes; that is, balloonborne ozonesondes that were found, returned, cleaned, and tested in the laboratory. Many reconditioned ozonesondes show excellent agreement (within ±1.5% of a TEI surface ozone calibrator) and compare well in dual ozonesonde flights with new instruments throughout the troposphere. However, about 25% of the reconditioned ozonesondes have measured 15 to 30 DU lower than the Dobson spectrophotometer. Dual ozonesonde flights, with new and reconditioned ozonesondes, have shown that the reconditioned ozonesondes often give low ozone values in the stratosphere. A linear normalization would result in a match in total column ozone that would skew the tropospheric measurements too high if height-dependent profile changes are not accounted for in the profile correction for reconditioned ozonesondes.

Since 1986 the ozonesondes flown at SPO have provided a detailed look at the yearly ozone hole development during mid-August to early October. Figure 4.3 shows the pre-ozone hole profiles measured during the winter compared to the minimum total column ozone observed. The 2003 ozone hole followed the typical severe depletion pattern, reaching the minimum total

Table 4.7. Summary of 2002-2003 Ozonesonde Projects

Ozonesonde Sites	2002 Totals	2002 Dates	2003 Totals	2003 Dates	Project
Station (weekly)					
Boulder, Colorado	53	Full year	57	Full year	NOAA long term
MLO	58	Full year	50	Full year	NOAA long term
SPO	65	Full year	81	Full year	NOAA long term
Fiji	27	Full year	31	Full year	PEM Tropics/SHADOZ
SMO	42	Full year	43	Full year	PEM Tropics/SHADOZ
Trinidad Head, California	71	Full year	47	Full year	NOAA "Health of the Atmosphere"
Huntsville, Alabama	48	Full year	50	Full year	NOAA "Health of the Atmosphere"
Galapagos	36	Full year	27	Full year	SOWER/SHADOZ
Intensives (~daily)					
Trinidad Head, California		April 19 – May 17			ITCT 2K2
South Pole (SPO)				June 15 – Oct. 15	QUOBI - additional ozonesondes

Table 4.8. Percent Difference [(Sonde – Dobson)/Dobson] Between Total Column Ozone from Ozonesondes and Dobson Spectrophotometers

Field Site	CMR	SBUV
Boulder	+2.2 ± 4.6	-1.1 ± 3.5
SPO	+2.0 ± 4.6	+4.6 ± 4.4
SMO	+0.3 ± 4.0	-5.4 ± 3.0
Hilo/MLO	+3.4 ± 4.1	-1.8 ± 3.3

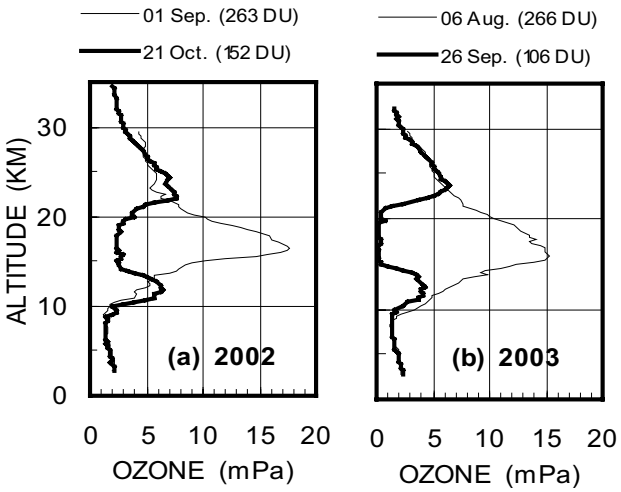

Figure 4.3. SPO ozonesonde profiles measured in (a) 2002 and (b) 2003 showing the pre-ozone-hole profile and the minimum total column ozone profile.

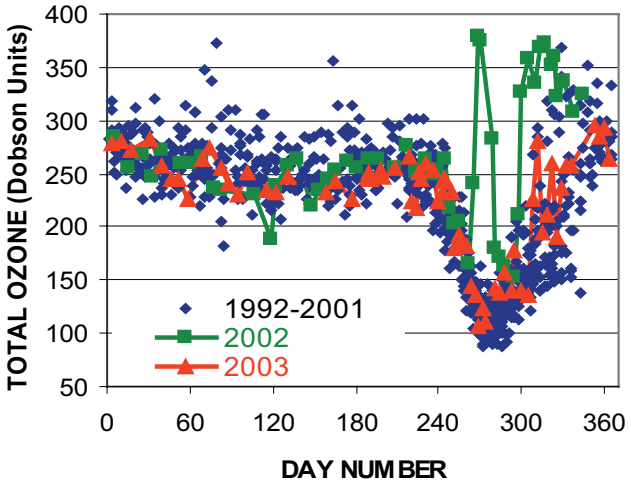

Figure 4.4. SPO total column ozone measured by ozonesondes during 1992-2001 compared to 2002 and 2003.

column ozone of 106 ± 5 DU on 26 September with near complete depletion in the 14- to 21-km layer. The previous year, 2002, was much different because a rare stratospheric warming event in the Southern Hemisphere forced an early breakup of the ozone hole. Total ozone was up to 378 DU on 25 September. This was far above the average in Figure 4.4 for that time period. The increase also coincides with a stratospheric temperature increase in the 20- to 24-km layer of over 50°C, rising from –80°C to over –30°C. The NOAA and NASA satellite observations showed the Antarctic polar vortex split in two at that time. Both vortices were displaced away from SPO. One of the vortices appeared to regain its position over SPO in early October and a minimum total ozone of 152 DU was observed on 21 October before total ozone increased rapidly again to more than 300 DU on 27 October 2002. Only 1988 is comparable to 2002 when measurements of the polar vortex resulted in a minimum total ozone value of 190 DU. Therefore, with the return of average ozone-hole conditions over SPO in 2003, there appears to be no immediate signs of long-term recovery.

4.1.6. Atmospheric Water Vapor

Water vapor measurements with balloonborne, frost-point hygrometers continued at Boulder, Colorado. The lower stratosphere was marked by relatively dry conditions during 2002-2003. This may be related to colder temperatures near the equatorial tropopause during that period [*Randel et al.*, 2004]. Campaigns were carried out in the Arctic and New Zealand as part of the Stratospheric Aerosol and Gas Experiment (SAGE) III

satellite validation activities. Also, campaigns were carried out at several locations with an emphasis on tropospheric profiles for the Atmospheric Infrared Sounder (AIRS) satellite validation.

4.1.7. ATMOSPHERIC TRANSPORT

Several enhancements that should improve the diagnosis of air parcel transport were made to the CMDL atmospheric trajectory model. The first improvement is the use of reanalysis data sets as input to the trajectory model. Ten years of National Centers for Environmental Prediction/National Center for Atmospheric Research (NCEP/NCAR) reanalysis data set (starting in 1993) were installed on disk. The plan is to acquire at least that much of the European Centre for Medium-Range Weather Forecasts (ECMWF) ERA-40 reanalysis data set. Both of these data sets have twice the temporal resolution and an increase in vertical resolution compared with the operational data sets previously used in CMDL with meteorological data grids available at 0, 6, 12, and 18 UTC. The reanalysis data are the best estimate of atmospheric conditions calculated by a state-of-the-art weather prediction model. The maximum number of quality-controlled global weather observations can be incorporated into the reanalysis data after the fact. Although there are no guarantees, these data sets represent a significant improvement over the operational products and will probably be used as the standard in the atmospheric research community. A trajectory comparison study will quantify differences in trajectories produced using the two reanalysis data sets. Although both data sets are available, the plan is to use the European reanalysis as the standard input.

The second improvement is the capability of producing three-dimensional (3-D) kinematic trajectories. These trajectories follow the winds in three directions according to the gridded wind fields (u, v, and w) output by the weather prediction model. The w, or omega, field provides the vertical wind velocity in pressure units of Pa s^{-1}. Because the vertical wind is not an observed quantity, it is derived by vertically integrating the horizontal wind divergence and dynamically balancing the result. A major source of uncertainty in the omega field is the parameterization of cumulus convection that comes into play in tropical latitudes and summertime midlatitudes. Although using the supplied vertical wind has become the preferred method for the calculation of trajectories, CMDL continues to offer isentropic trajectories as well as 3-D trajectories. A study comparing trajectories calculated by the two methods is ongoing. Preliminary results appear in Section 4.2.4.

The 3-D model has a 1-hour time step. The integration is done by the second-order Runge-Kutta or Midpoint Method [*Press et al*., 1992]. In equation form:

$$k_1 = hf'\left(x_n, y_n\right)$$

$$k_2 = hf'\left(x_n + \frac{1}{2}h, y_n + \frac{1}{2}k_1\right)$$

$$y_{n+1} = y_n + k_2$$

where *f'(x,y)* is the wind velocity at time *x* and position *y* and *h* is the time step.

Given a starting latitude, longitude, and elevation (z_0) the first step is to find a corresponding initial pressure, p_0. This is done by knowing the Kelvin temperature, T, on the pressure surfaces above and below the initial elevation, z_0, and assuming T varies as p, integrating the hydrostatic equation from the lower pressure level and iterating to solve for p_0 using the Newton-Raphson method [*Stark*, 1970]. Here $K = R/c_p$, where R is the gas constant and c_p is the specific heat of air at constant pressure. The u, v, and w wind velocities to be used in the advection step are determined by bilinearly interpolating the winds on the two pressure surfaces that bracket z_0. The wind velocities are then assumed to vary linearly with height.

Latitude, longitude, pressure, temperature, and elevation are reported for each 1-hour position along the trajectory. The latitude, longitude, and pressure are determined by advecting the air parcel for 1 hour using the u, v, and w winds in the aforementioned scheme. The temperature is determined between the two bracketing pressure surfaces by assuming that it varies as p^K. The new elevation in meters is found by integrating the hydrostatic equation from the lower mandatory pressure level to the new pressure level.

4.1.8. STRATOSPHERIC AEROSOLS

The Nd:YAG lidars at MLO and Boulder continued to operate with weekly observations throughout 2002-2003. The scientific purpose behind the weekly observations is to conduct accurate simultaneous ozonesonde and aerosol measurements at the two sites during the next major volcanic eruption. At that time, large effects on ozone are expected because of the added aerosol surface area and a maximum level of chlorine. Although another year at background levels was experienced, a major eruption remains a possibility at any time.

Stratospheric aerosols over MLO continue at the background level first attained in 1996 (over 8 years ago); it is the longest background period since the stratospheric aerosol layer was discovered in June 1959. The seasonal variation in the background level, discovered in 1999, continues with a maximum during the winter when transport from the tropics is expected. This suggests a tropical source for the background aerosol. In Figure 4.5 the integrated aerosol backscatter (IABS) is shown for both MLO and Boulder. The entire stratospheric layer is integrated in the case of MLO, but only the upper part of the layer is integrated over Boulder. The tropopause varies in altitude so much at Boulder that integrating only the upper portion gives a better correlation with the MLO data. *Autuna et al.* [2002, 2003] present global studies of the Pinatubo eruption using MLO data sets, other lidar data sets, and SAGE satellite measurements. Several observations at both MLO and Boulder measured aerosol peaks above the tropopause. These were probably caused by small eruptions that added only a fraction of aerosol to the background layer and were identifiable for only a few weeks at a time.

The new lidar for SMO was constructed and is now being tested in Hawaii. An abandoned NWS building in Pago Pago, American Samoa, was procured to house the lidar. This enables the CMDL staff living in Pago Pago to make evening observations without driving the circuitous 25-mile road to the observatory. After the SMO lidar installation is complete, there

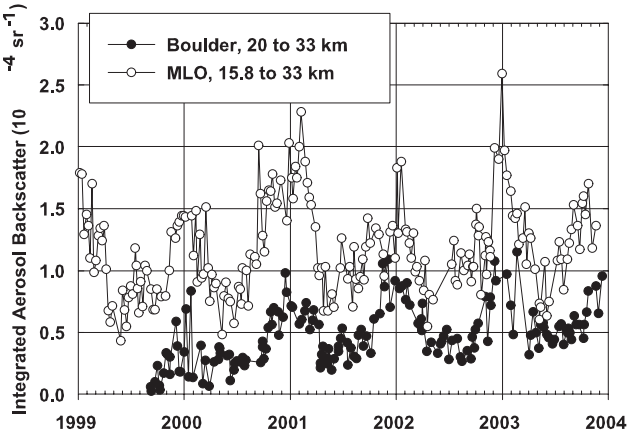

Figure 4.5. Lidar measurements of integrated aerosol backscatter for the stratosphere. At MLO the altitude range is 15.8 to 33 km; at Boulder the range is 20 to 33 km.

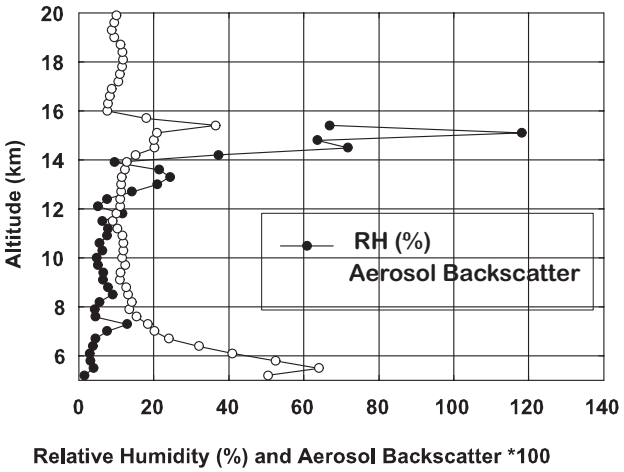

Figure 4.6. Lidar measurement made on 2 October 2002 of water vapor and aerosol backscatter (532 nm) at MLO.

will be active monitoring lidars at 40°N, 19°N, 14°S, and 45°S (Lauder, New Zealand) that bracket the important tropical region.

A campaign to compare ozone and temperature measurements was conducted in August 2002 at MLO. The NASA Goddard mobile lidar was deployed and additional ozonesondes were launched from Hilo. The Jet Propulsion Laboratory (JPL) lidar at MLO measured ozone and temperature. The MLO Dobson, the world standard Dobson, and the microwave ozone instrument were also used in the campaign. A scientist from NASA Goddard was the referee for the campaign. The MLO, Goddard, and JPL lidars were able to measure temperature from 30 to 70 km simultaneously. Above 50 km the three measurements agreed to within 1°C, but below 50 km the MLO lidar showed a systematic shift of 1°C-2°C. This discrepancy is under investigation.

Channels were added to the MLO lidar in 2001 to detect Raman scattering from water vapor in the free troposphere. A 2-year proposal to validate the water vapor measurement by the AIRS instrument [*Fetzer et al*., 2003] on the AQUA satellite was funded by NASA. The grant was used to improve the lidar's measurement system by adding detectors, a larger mirror (74 cm), and to calibrate it with balloon water vapor measurements launched from the observatory. CMDL frost-point hygrometers, capable of measuring stratospheric water vapor, were launched from Hilo as part of the validation [*Vömel et al.*, 2003]. Figure 4.6 is an example of a water vapor profile along with the aerosol backscatter at 532 nm. The observation taken on 2 October 2002 shows the typical dry upper troposphere (relative humidity (RH) below 20%) measured with the water-vapor channels as well as a wetter layer between 14 and 16 km. The wetter layer corresponds to subvisible cirrus, a common phenomena easily seen by the 532-nm aerosol channel. The aerosol backscatter attains values greater than the 0.1 background, peaking at about 0.4 in the wet layer. These elevated values of aerosol backscatter indicate condensation and are often seen when the relative humidity is not exactly saturated (RH of 100% expected for equilibrium conditions). In this profile there are four points in the layer with an RH of 70% (undersaturated) and one with an RH of 120% (supersaturated). These may indicate nonequilibrium conditions because of transport, temperature changes, or differences in the abundance of condensation nuclei.

An innovation on the standard lidar technique was developed to measure boundary layer aerosols. The technique (CLidar) uses a change-coupled device (CCD) camera to image the entire laser beam (90°) from a few hundred meters away. The method has very high altitude resolution in the boundary layer, can measure accurately all the way to ground, and is a relatively simple instrument; *Barnes et al*. [2003] describe the technique. A proposal in collaboration with Central Connecticut State University was funded by the National Science Foundation (NSF) to develop an instrument that can be used by the CMDL aerosol group for both long-term monitoring and campaign monitoring of boundary layer aerosols. A second generation camera system will be built for the CLidar with a much higher light gathering power. The system will be portable and able to measure aerosols with a much smaller laser than the one in the present system.

4.2. Special Projects

4.2.1. Water Vapor Instrument Development

The cryogenic frost-point hygrometer used by CDML is based on a design in the work of *Mastenbrook and Dinger* [1960] with only one major change in 1979 when the stratospheric monitoring program was moved from the Naval Research Laboratory (NRL) to CMDL in Boulder. This instrument has been one of the most important tools for stratospheric water vapor measurements and has contributed significantly to our understanding of stratospheric water vapor [*Oltmans and Hofmann,* 1995; *Vömel et al.,* 1995, 2002]. The instrument is limited due to its design, which includes measurements of both stratospheric and upper tropospheric water vapor with upper tropospheric measurements being slightly less reliable than stratospheric measurements. Furthermore, the design led to some variability in the performance as well as some shortcomings in the availability.

In cooperation with the Cooperative Institute for Research in Environmental Sciences (CIRES) at the University of Colorado (CU), a new cryogenic frost-point hygrometer (CFH), based on the CMDL frost-point hygrometer, was developed to overcome some of the limitations of the older instrument and at the same time reduce power consumption and weight. The CU-CFH instrument also requires less skill to operate, thus facilitating data acquisition in the network for the detection of stratospheric and upper tropospheric water vapor.

Important features of the CU-CFH instrument are:

- The same cryogenic cooling system as the CMDL frost point hygrometer
- Optimized optical condensate detection
- Microprocessor controlled
- Pulse-width modulated heater
- Digital interface with ozonesonde
- Weight < .6 kg (1.5 lb) including batteries and cryogen
- Improved mirror calibration
- No condensate ambiguity
- Simplified instrument preparation and setup

The major components of the CU-CFH instrument are the mirror assembly with integrated heater and thermistor, the optical sensor, and the microprocessor controller (Figure 4.7). The exposed end of the mirror assembly is installed in the cryogen container (not shown).

The microprocessor control allows an enhanced feedback control loop to maintain a constant frost layer, a method designed to avoid condensate phase uncertainties, and allows other flexible control routines. The electrical requirements of this instrument are 70% below the old CMDL hygrometer, which translates into a savings in weight and balloon size.

The thermistor resistance is measured by the microprocessor and converted into a temperature using the individual calibration coefficients. This reduces the susceptibility to radio frequency interference and allows the transmission of control values to check further processing errors. Data transmission is done through digital communication with an ENSCI V2D interface board. The mirrors are calibrated against a National Institute of Standards and Technology (NIST) traceable reference temperature probe in the range from –85°C to +20°C that can easily be extended down to –95°C thus eliminating any extrapolation errors below the conventionally used lowest calibration point of –79°C.

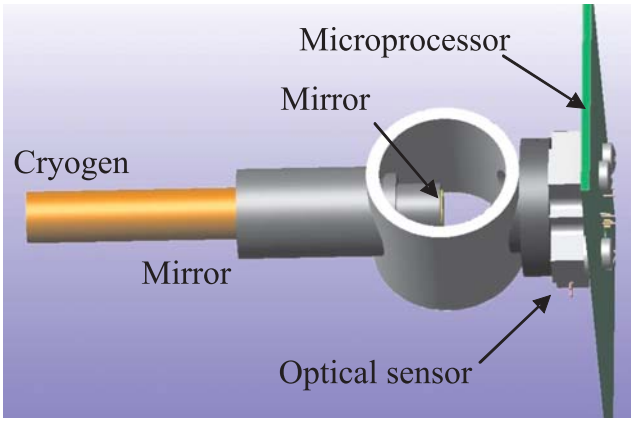

Figure 4.7. Schematic of the CU-CFH sonde. The mirror assembly to the left of the sample volume ring is installed in the cryogen storage container and normally is not visible. The exposed part on the left of the mirror assembly is in contact with the cryogen cooling the mirror. The heater is inside the mirror assembly and is not shown. The thermistor measuring the mirror temperature is embedded in the mirror and also is not shown. Both heater and thermistor are connected to the controller to the right of the optical sensor.

CU-CFH sondes are flown with ozonesondes and were used in 5 test soundings at Boulder, 12 soundings during Atmospheric Infrared Sounder Water vapor Experiment (AWEX) at the Atmospheric Radiation Measurement (ARM)/Cloud and Radiation Testbed (CART) site near Lamont, Oklahoma, and in 4 soundings during the third Soundings of Ozone and Water in the Equatorial Region (SOWER) field campaign at Bandung, Indonesia. There is very good agreement between the CFH sonde and the Vaisala RS80-H radiosonde that produces reliable data in this altitude range of the lower troposphere. The excellent performance of the CU-CFH sonde in the lower troposphere is shown in Figure 4.8. The Snow White hygrometer shows some disagreements below 6 km. Because there are no comparison soundings in the stratosphere, only one sounding is shown in Figure 4.9. This profile shows 1.2-second resolution raw data between the surface and 28 km and demonstrates the capabilities of the CFH sonde between the lower troposphere and middle stratosphere. The continuously adjusting controller parameters eliminate data gaps because of gain changes and clear pulses.

In the lower troposphere frost-point instruments deal with an inherent ambiguity in the phase of the condensate on the mirror. Instruments like CU-CFH or Snow White can maintain liquid water as condensate on the mirror down to temperatures of –25°C to –30°C. The transition from liquid-to-frozen condensate happens spontaneously at temperatures that vary for each sounding. Therefore, insufficient knowledge concerning the phase of the condensate may lead to an incorrect calculation of the water vapor pressure because the phase of the mirror condensate (liquid or solid) determines the vapor pressure curve used to calculate the partial pressure of water in the air above the mirror. This ambiguity explains the disagreement between Snow White and CU-CFH measurements below 6 km shown in Figure 4.8. The CU-CFH control algorithm removes the liquid/ice ambiguity; however, the comparison of the two sensors shows that the calculation of RH from the Snow White frost-point measurements uses the wrong vapor pressure equation (ice) below 6 km. Therefore, removing the ambiguity is of critical importance. The CU-CFH control algorithm eliminates the ambiguity at a temperature of –10°C, creating a data gap of typically 200 m or less and allows a clear identification of the condensate phase that is picked up in the data processing.

4.2.2. Arctic Water Vapor Measurements

During the winter of 2002 and 2003, a total of 11 frost-point hygrometers were launched in the Arctic at three different locations in cooperation with the Finnish Meteorological Institute (FMI) and the Alfred Wegener Institute (AWI). These soundings were part of the second SAGE III ozone loss and validation experiment (SOLVE2). Five soundings were launched at

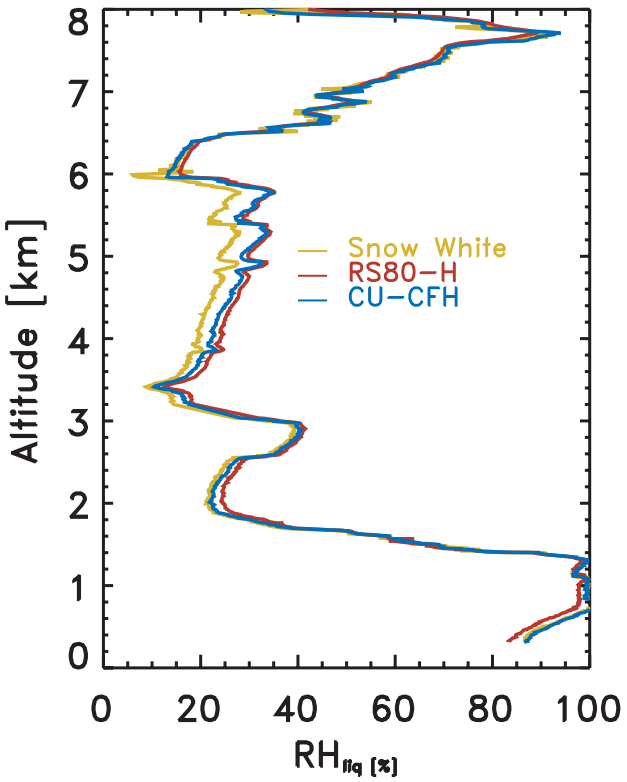

Figure 4.8. A sounding on 11 November 2003 at the ARM/CART site shows an excellent agreement between the CU-CFH sonde and the Vaisala RS80-H sonde in the lower troposphere using 1.2-second resolution data. The slight disagreement between the CU-CFH and the Snow White hygrometer below 6 km is due to the ambiguity in the phase of the mirror condensate in the Snow White instrument. This figure assumes ice on the mirror, which is an incorrect assumption for the Snow White below 6 km in this example. Using the appropriate liquid vapor pressure formulation in this region would bring all three instruments into agreement.

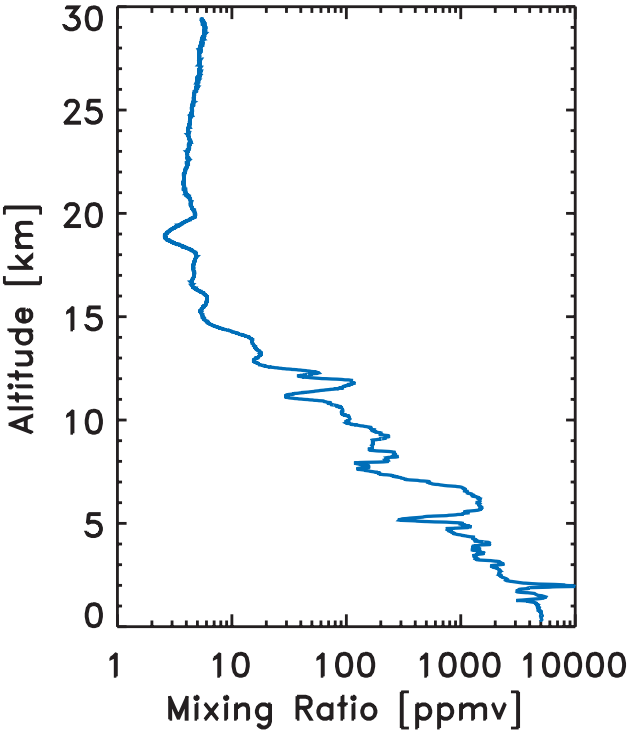

Figure 4.9. The ARM/CART site 1.2-second resolution CFH data between the surface and 28 km from a sounding on 7 November 2003.

Sodankylä, Finland; three at Esrange near Kiruna, Sweden; and three at Ny-Ålesund, Spitsbergen, Norway. The soundings at Sodankylä also carried ozonesondes, giving additional information about the air mass composition.

During AWEX the CU-CFH instrument was used to evaluate the performance of other radiosonde sensors, i.e., the Vaisala RS80, RS90, and RS92 radiosondes as well as the Meteolabor Snow White hygrometer. Only the comparisons with the Vaisala RS92 are shown in Figure 4.10. These are the first Vaisala RS92 soundings launched in North America. The comparisons show a very good agreement between these sensors with mean differences less than 3% RH throughout the entire troposphere. A small drying of the Vaisala RS92 values compared to the CU-CFH between the surface and 10 km is currently under investigation.

All stratospheric water vapor profiles are shown in Figure 4.11. With the exception of the last sounding at Sodankylä on 4 April 2003, all soundings show a very similar structure indicative of the interior of the vortex. Below 22 km some soundings show evidence of midlatitude transport.

The soundings were timed to coincide with SAGE III overpasses to provide independent validation measurements for the SAGE III satellite water vapor retrievals. The comparisons generally show a very good agreement between the preliminary SAGE III and CMDL frost-point water vapor profiles (Figure 4.12). The Kiruna sounding on 12 January 2003 shows higher water vapor values between 12 and 18 km compared to the SAGE III retrieval. This overpass event was close to Sodankylä and about 250 km east of Kiruna, which make inhomogeneities of the vortex an unlikely explanation for this discrepancy. The frost-point sounding encountered a cloud layer beginning at 2 km and measured ice saturation up to the tropopause. Therefore, it is probable that the intake tubes were contaminated in this region and caused additional water vapor to appear in the measurement. After drying the intake tubes (above 18 km) this sounding shows a good agreement with the SAGE III retrieval.

On 16 January 2003 the first direct comparison was made between the Laboratorie de Meteorologie Dynamique, Centre National de Recherche Scientifique, France (LMD) frost-point

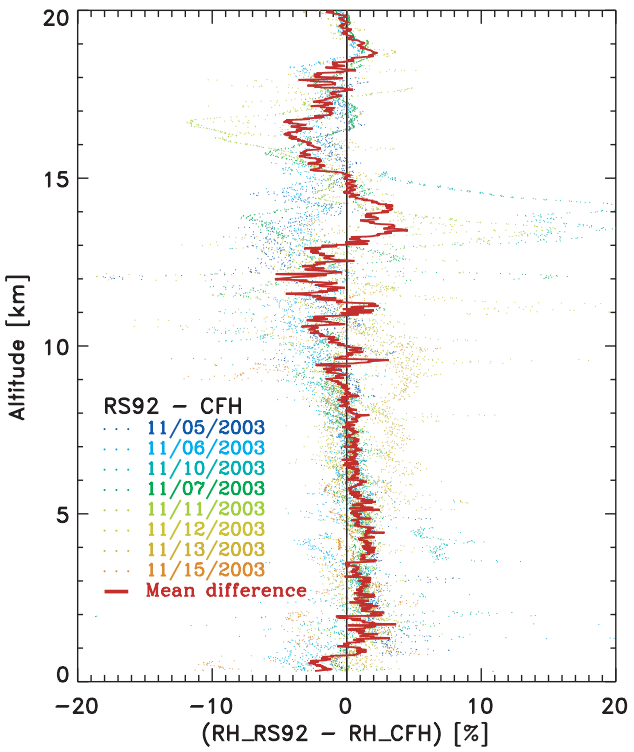

Figure 4.10. Mean relative humidity difference between the Vaisala RS92 radiosonde humidity sensor and the CFH relative humidity from eight soundings during AWEX, 5-15 November 2003.

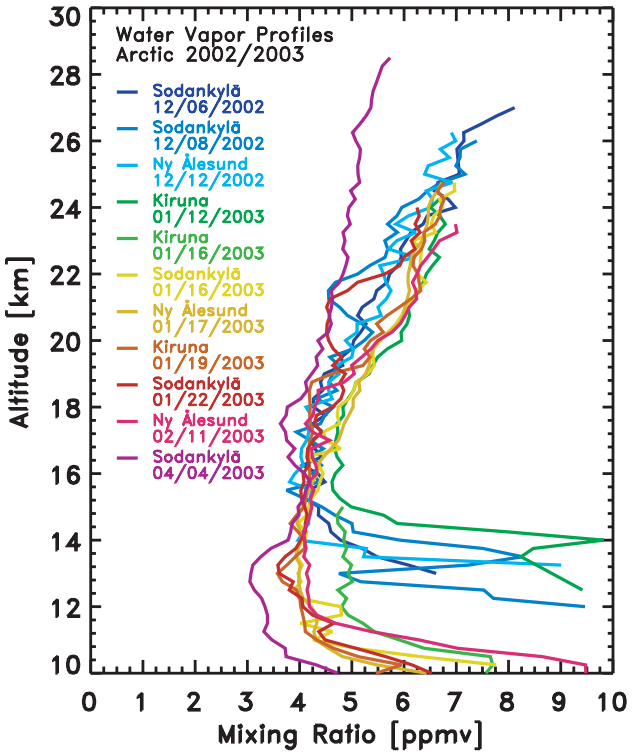

Figure 4.11. Summary of all Arctic soundings in the winter 2002 and 2003. Sounding sites are Ny-Ålesund, Norway; Spitzbergen, Norway; Kiruna, Sweden; and Sodankylä, Finland. Above 22 km all soundings before April show high values characteristic of vortex air.

hygrometer [*Ovarlez*, 1989] and the CMDL frost-point hygrometer (Figure 4.13). The LMD hygrometer was launched at Kiruna, Sweden, and a CMDL hygrometer was launched on the same day at Sodankylä, Finland, about 400 km to the east of Kiruna. A second CMDL hygrometer was launched at Esrange, but produced reliable data only up to 12 km. At Ny-Ålesund (79°N, 12°E) a third CMDL hygrometer was launched on 17 January 2003. All soundings were launched well inside the vortex and show remarkably similar profiles at all altitudes above 10 km. The agreement between the LMD and the CMDL hygrometer indicates that there is no systematic bias between these two instruments. The excellent agreement with the Ny-Ålesund sounding, launched 1 day later and roughly 1300 km further north, indicates the water vapor distribution in the interior of vortex is remarkably homogenous in the absence of large-scale dehydration.

In early December 2002 the vortex was centered over northern Scandinavia and exhibited very cold temperatures. The sounding at Sodankylä on 6 December 2002 showed some layers of saturation in the stratosphere, but no significant reduction in water vapor was found (Figure 4.14). The sounding at Sodankylä 2 days later shows a shallow layer of lower water vapor between 475 and 500 K and another layer of lower water vapor between 510 and 560 K (Figure 4.15). These layers are either remnants of dehydration or an indication of midlatitude transport. The Modele Insentrope du transport Meso-echelle de l'Ozone Stratospherique par Advection (MIMOSA) model created a vertical cross section of modified potential vorticity (PV) at 27° longitude that roughly corresponds to the balloon trajectory. This PV cross section (Figure 4.16) shows the transition from midlatitude to vortex air occurred between 475 and 500 K. The lower of the two layers is clearly of midlatitude origin. A similar event was observed at Ny-Ålesund on 22 January 2003 and is discussed in detail in the work of *Müller et al.* [2003]. The upper layer between 510 and 560 K, on the other hand, is clearly vortex air. A trajectory analysis at 550 K shows that the temperatures in this layer were cold enough for ice particle formation and removal of water. Thus the slightly lower water vapor concentration observed in this layer is the result of dehydration and similar to the event observed at Sodankylä in January of 1996 [*Vömel et al.*, 1997]. Nevertheless, it is remarkable to observe this kind of event very early in the winter.

4.2.3. Stratospheric Water Vapor Campaigns

Table 4.9 lists the CMDL/CU water vapor campaigns for 2002 and 2003. These campaigns used the CMDL frost-point hygrometer or the new CU-CFH instrument to measure stratospheric and upper tropospheric water vapor. The water vapor campaigns were to validate the AIRS instrument onboard the AQUA satellite, to validate the SAGE III instrument onboard the Meteor-3M satellite, to study the tropical upper tropospheric

Table 4.9. Stratospheric and Upper Tropospheric Water Vapor Campaigns

Site	Date	Number of Soundings	Project	Instruments
Watukosek, Indonesia	Dec. 2001	6	SOWER	CMDL-FP, ECC, SW, RS80
Hilo, Hawaii	March 2002-March 2003	2	AIRS validation	CMDL-FP, ECC, SW, RS80
San Cristóbal, Galapagos	Aug. 2002-March 2003	3	AIRS validation	CMDL-FP, ECC, SW, RS80
Huntsville, Alabama	Nov. 2002	2	AIRS validation	CMDL-FP, ECC, SW, RS80
Sodankylä, Finland	Dec. 2002-April 2003	5	SAGE III validation	CMDL-FP, ECC, SW, RS80
Ny Ålesund, Norway	Dec. 2002-Jan. 2003	4	Arctic	CMDL-FP, RS80
Kiruna, Finland	Jan. 2003	3	SAGE III validation	CMDL-FP, RS80
Watukosek, Indonesia	Jan. 2003	4	SOWER	CMDL-FP, ECC, SW, RS80
Lauder, New Zealand	March-Nov. 2003	4	SAGE III validation	CMDL-FP, ECC, SW, RS80
San Cristóbal, Galapagos	July 2003	3	AIRS validation	CMDL-FP, ECC, SW, RS80
ARM/CART, Oklahoma	Oct.-Nov. 2003	12	AWEX	CU-CFH, ECC, SW, RS80, RS92
Bandung, Indonesia	Dec. 2003	4	SOWER	CU-CFH, ECC, SW, RS80
Ny Ålesund, Norway	Dec. 2003	1	Arctic	CMDL-FP, RS80

Instruments: CMDL-FP, CMDL frost-point hygrometer; ECC, electrochemical concentration cell; SW, Snow White hygrometer (Meteolabor), ozonesonde; RS80; Vaisala RS80; CU-CFH, University of Colorado cryogenic frost-point hygrometer.

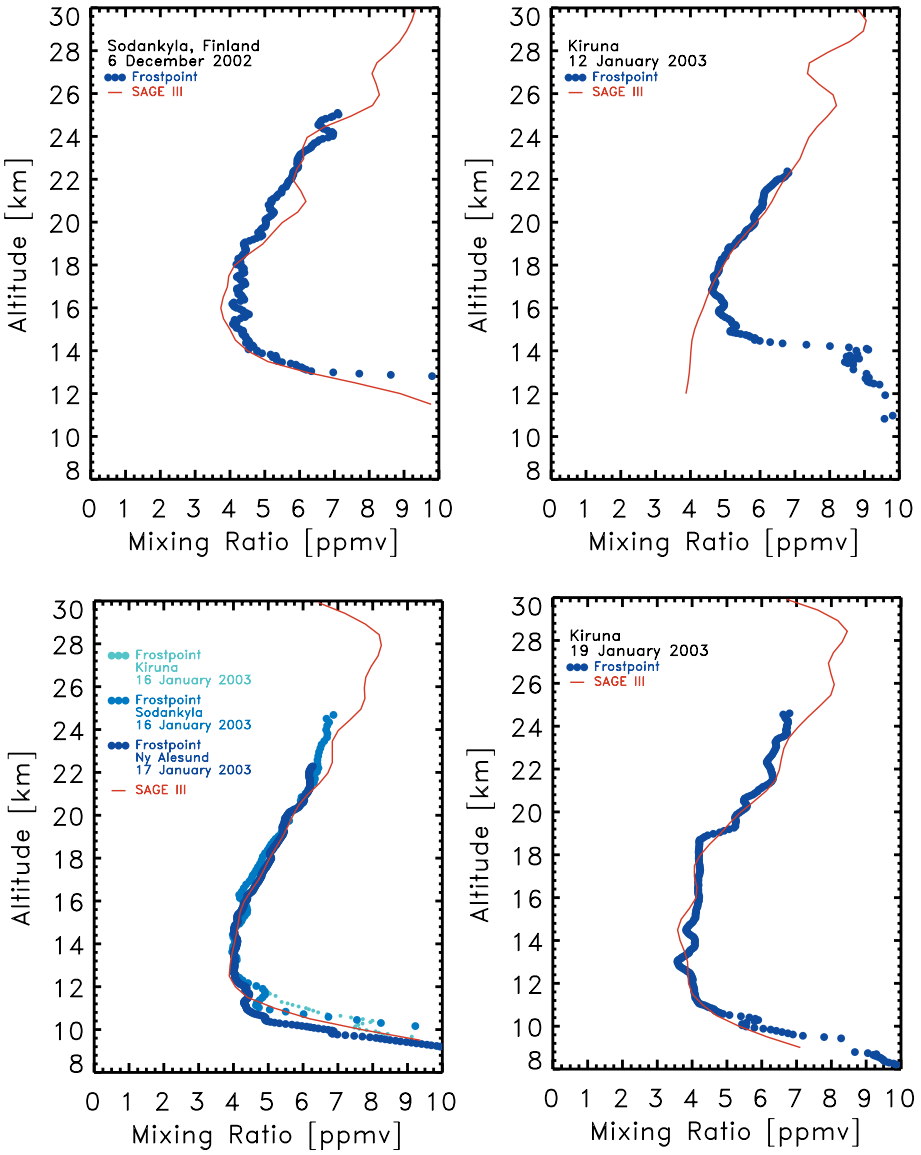

Figure 4.12. Comparison between SAGE III retrieval and CMDL frost-point water vapor profiles.

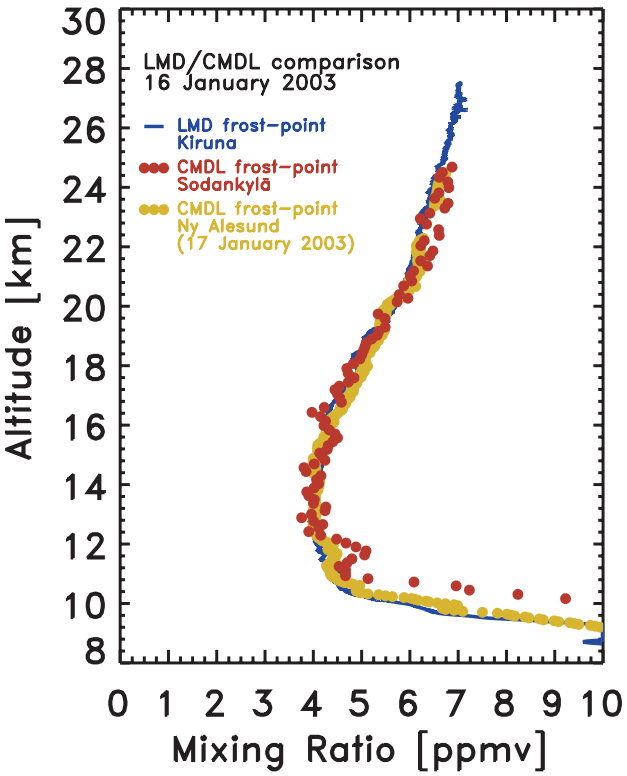

Figure 4.13. Comparison between the LMD frost-point hygrometer and the CU/CMDL frost-point hygrometer showing excellent agreement between the instruments flown on 16 January 2003 at Kiruna, Sweden, and Sodanklylä, Finland, and on 17 January 2003 at Ny-Ålesund, Norway.

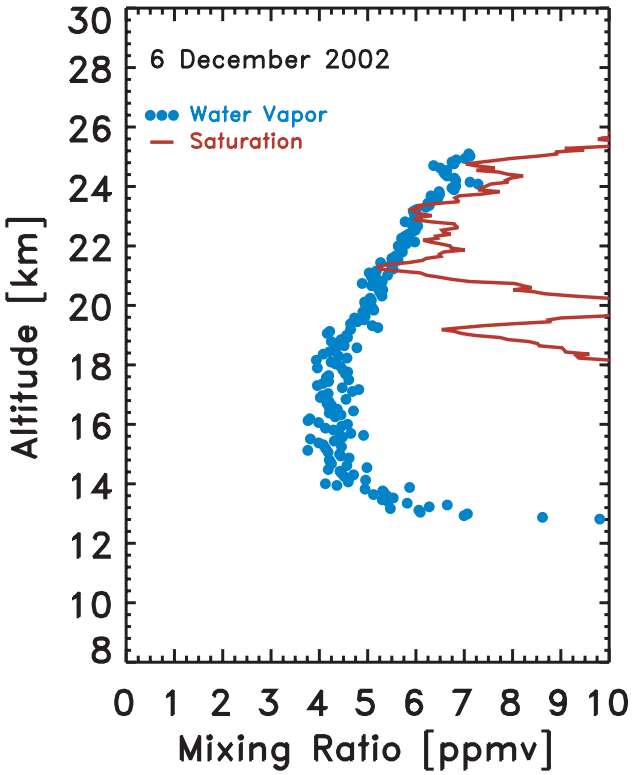

Figure 4.14. Water vapor and saturation mixing ratio profiles at Sodankylä, Finland, 6 December 2002. Note some shallow layers of saturation between 21 and 25 km.

and lower stratospheric water vapor, and to validate a number of different radiosonde humidity sensors. Each campaign typically lasted between 5 days and 2 weeks except for the campaign at the ARM/CART site that lasted 3 weeks.

The soundings at Lauder, New Zealand; San Cristóbal, Galapagos; Sodankylä, Finland; Hilo, Hawaii; and Ny-Ålesund, Norway, were launched in cooperation with local personnel. Also, personnel from the site at Watukosek, Indonesia, were trained to fly the CU-CFH sondes during the Bandung, Indonesia, campaign, and the AWI scientist, who launched the sondes at Ny-Ålesund, was trained during the campaign at Sodankylä. Additional sondes were launched by the local staff after the completion of the campaigns. These stations form the basis for a proposed network of water vapor sounding sites. They span the region between the high Arctic and the southern midlatitudes and will allow for long-term observations of stratospheric and upper tropospheric water vapor by in situ measurements. These sites will continue to play a major role in the validation of satellite instruments.

AWEX focused on the intercomparison of different radiosonde humidity sensors used in the validation of the AIRS instrument. In addition to the sondes listed in Table 4.9, radiosondes made by Sippican and Intermet as well as Vaisala RS90 radiosondes were launched on a separate balloon. The instruments used during AWEX listed in Table 4.9 were launched on the same balloon and provide the best database for this experiment. Some results are shown in Figure 4.10.

Most soundings included the Snow White hygrometer. These measurements, along with the strengths and weaknesses of this instrument, appear in the works of *Fujiwara et al.* [2003] and *Vömel et al.* [2003]. The observations at the tropical sites appear in the work of *Vömel et al.* [2002].

4.2.4. Sensitivity of Isentropic and 3-D Trajectories to Temporal Interpolation

As part of an ongoing investigation of the differences among various trajectory types, a study quantifying the effects of temporal interpolation on isentropic and 3-D trajectories is presented here. The NCEP/NCAR reanalysis data set in the format of 2.5° latitude/longitude grids was used as meteorological input data.

Trajectories were calculated for 1 year (2001) at three different sites: Alert, Canada (ALT); MLO; and a site in Oklahoma called the Southern Great Plains (SGP). Arrival elevations were 3000 m for ALT, 3400 m for MLO, and 1000, 2000, and 3000 m for SGP. The three arrival levels for SGP were chosen to determine the effect of elevation (hence wind speed) on trajectory differences.

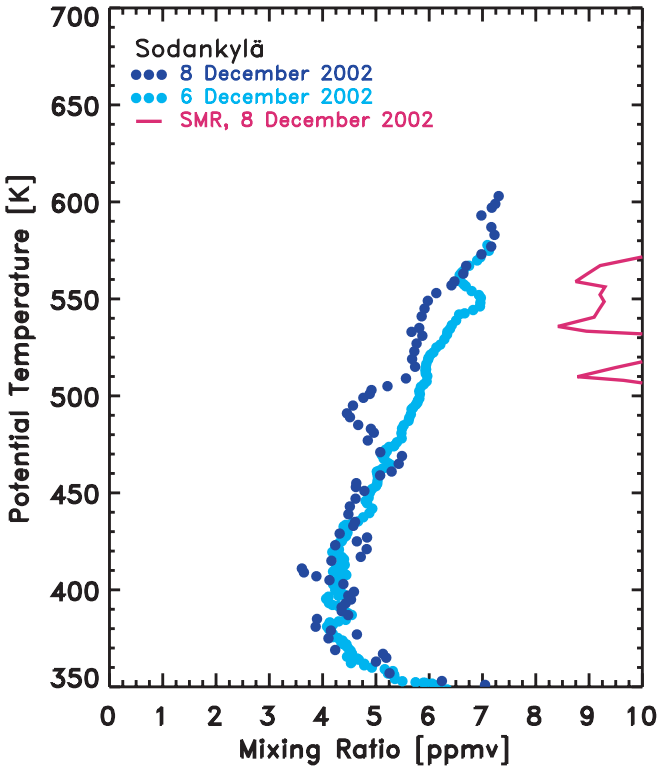

Figure 4.15. Water vapor profiles on 8 December 2002 at Sodankylä, Finland, compared to the sounding 2 days prior. Also shown is the saturation mixing ratio for the sounding on 8 December 2002.

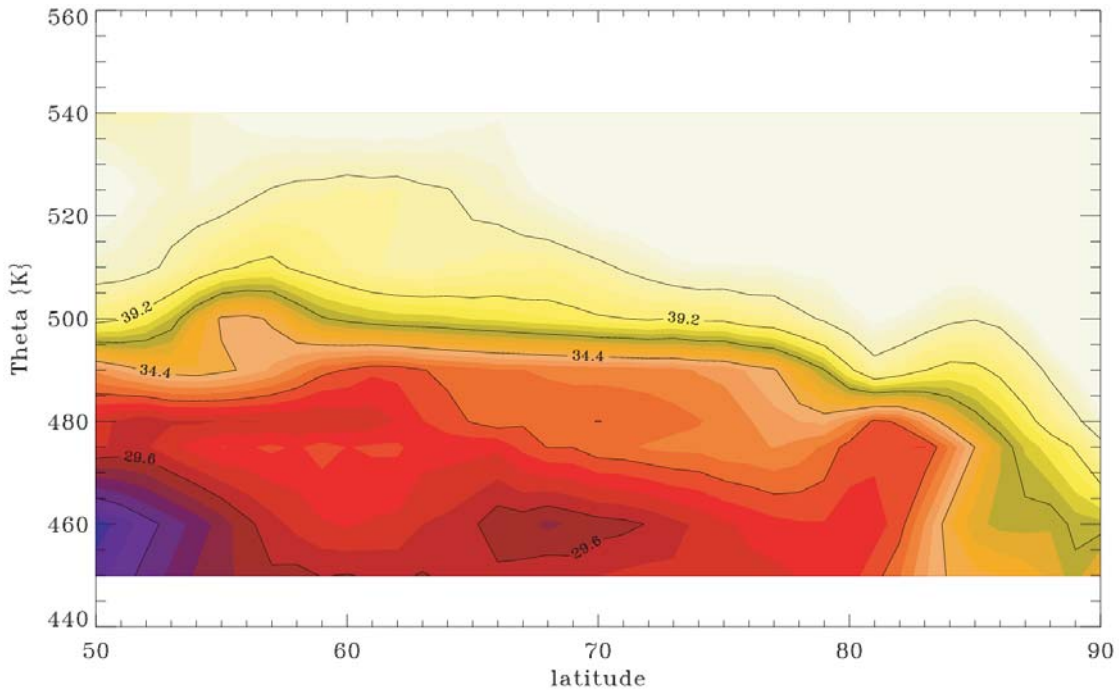

Figure 4.16. Vertical cross section of modified PV at 27° longitude corresponding to the balloon trajectory shows the transition from midlatitude to vortex air between 475 and 500 K. Red and blue colors indicate midlatitude air, light colors indicate vortex air. This transition corresponds to the lower of the two layers showing reduced water vapor. Sodankylä, Finland, is at 67°N.

In this study trajectories are calculated from the full data set that has meteorological grids for 0, 6, 12, and 18 UT (referred to hereafter as "true trajectories") and compared with trajectories calculated from a temporally sparse data set with grids at 0 and 12 UT only (referred to hereafter as "interpolated trajectories").

Figures 4.17 and 4.18 show the statistics for isentropic trajectories. The average horizontal transport difference (AHTD, Figure 4.17) is the distance between the true trajectory and the interpolated trajectory given at 3-hour intervals along the trajectory. The distance was calculated by spherically rotating the true position to the North Pole and then the interpolated position was rotated with respect to it. The transport difference in kilometers is calculated simply as $(90 - \text{lat}_s) \times 111.1984$, where lat_s is the latitude of the rotated position of the interpolated trajectory. Figure 4.17 shows that after 96 hours the AHTD range is 300-530 km with trajectories for SGP at 3000 m giving the greatest difference, while MLO trajectories produce the least horizontal transport difference because of temporal interpolation. As might be expected, the AHTDs for SGP range from smaller to larger for trajectories arriving at elevations from 1000 to 3000 m. The horizontal transport differences result from errors in the u and v wind caused by the temporal interpolation. The vertical position error also contributes to the AHTD because of the vertical gradient usually present in the horizontal wind speed. For example, higher wind speeds at higher elevations cause the differences to be greater.

The statistic presented in Figure 4.18 is the signed vertical transport difference (SVTD) which is the average (for 2001) of the vertical distance between the true trajectories and their interpolated counterparts. This statistic is also reported at 3-hour intervals out to 96 hours. For isentropic trajectories the vertical level of the air parcel is determined by the elevation of the isentropic surface, which, in turn, depends on temperature, T, and pressure, p, as shown in the formula for potential temperature, $\Theta = T \times (1000/p^{K})$. Interpolation errors in T and/or p could cause errors in the level of the isentropic surface. For instance, if the interpolated T is colder than the actual T, the isentropic surface would have a higher elevation than it should have. The sawtooth pattern in the SVTD (Figure 4.18) requires an explanation. When the temporal interpolation occurs at hours 6 and 18 UT, the trajectories drift apart while at 0 and 12 UT (with real data constraining the level of the isentropic surfaces) the true and interpolated trajectories have elevations that are closer to each other. The sawtooth pattern is less pronounced at ALT than the other sites, perhaps because the more stable atmosphere there leads to less vertical motion to begin with. Also, during the course of the year at ALT there is less diurnal variability in temperature that results in smaller interpolation errors.

It is instructive to compare the effect of temporal interpolation in isentropic trajectories to the effect in 3-D trajectories. Figures 4.19 and 4.20 present the same statistics, AHTD and SVTD, this time using 3-D trajectories. As seen in Figure 4.19, the AHTDs are significantly higher than the isentropic trajectories, ranging from 480 to 730 km after 96 hours. Although temporal interpolation affects the horizontal winds similarly in the 3-D case as in the isentropic case, there is a big difference in how temporal interpolation affects the vertical level of the two trajectory types. In the isentropic case, the level of the interpolated trajectories is constrained to one that is close to the true trajectories when real data are present (0 and 12 UT).

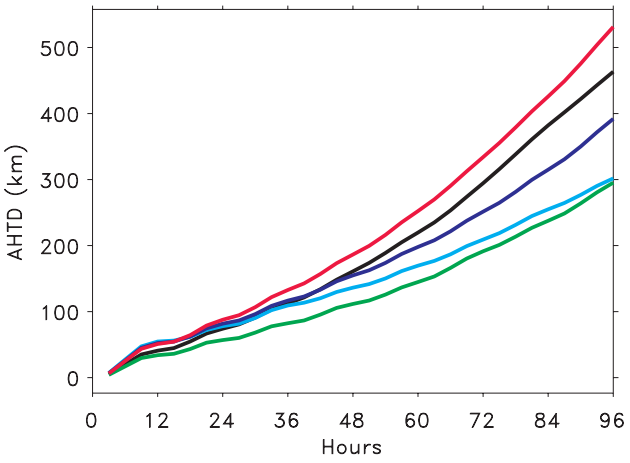

Figure 4.17. Average horizontal transport differences between true and interpolated isentropic trajectories for ALT, 3000 m (black), MLO, 3400 m (green), and SGP, 1000 m (aqua), 2000 m (blue), and 3000 m (red).

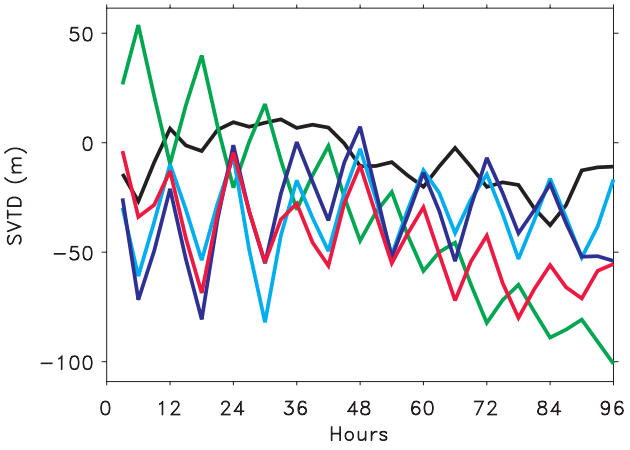

Figure 4.18. Signed vertical transport differences between true and interpolated isentropic trajectories for ALT, 3000 m (black), MLO, 3400 m (green), and SGP, 1000 m (aqua), 2000 m (blue), and 3000 m (red).

Therefore the vertical differences for isentropic trajectories stay small, 50-100 m after 96 hours (Figure 4.18). As shown in Figure 4.20, the vertical differences after 96 hours for 3-D trajectories are at least four times greater except for ALT. For 3-D trajectories, once the elevation of the interpolated trajectory diverges from the true trajectory, there is nothing to bring it back to the true level. In fact, the vertical gradient in the omega field may ensure that the interpolated trajectory continues to diverge vertically from the true one. At Alert the stability of the air (little vertical motion) keeps the interpolated trajectories close to the level of the true trajectories. However, at the other sites where there is more vertical motion, especially during daytime hours, the temporal interpolation has the effect of causing a significant error in vertical level over time. This, in turn, contributes to the horizontal differences seen in Figure 4.19. These results point out

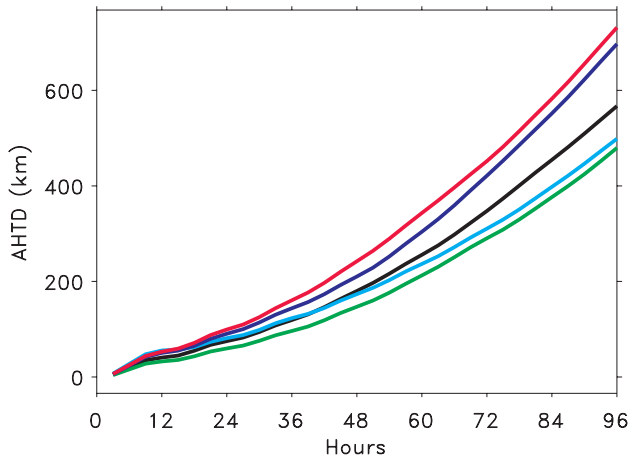

Figure 4.19. Average horizontal transport differences between true and interpolated 3-D trajectories for ALT, 3000 m (black), MLO, 3400 m (green), and SGP, 1000 m (aqua), 2000 m (blue), and 3000 m (red).

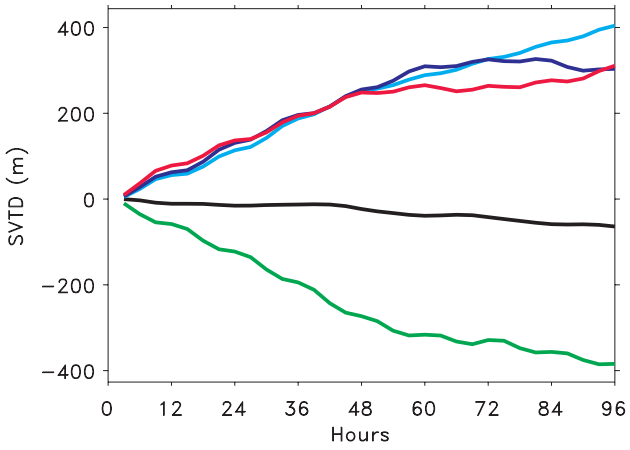

Figure 4.20. Signed vertical transport differences between true and interpolated 3-D trajectories for ALT, 3000 m (black), MLO, 3400 m (green), and SGP, 1000 m (aqua), 2000 m (blue), and 3000 m (red).

why isentropic trajectories may be preferable to 3-D trajectories when input grids are temporally sparse.

4.2.5. Tropospheric Ozone at Trinidad Head, California

In April 2002 surface ozone observations began at the newly established Trinidad Head, California, CMDL baseline observatory (THD). Prior to that time (since August 1997) regular weekly ozone launches were performed by nearby Humboldt State University Marine Sciences Laboratory at Trinidad Head. The beginning of the surface ozone measurements at THD coincided with the start of the Intercontinental Transport and Chemical Transformation 2002 (ITCT 2K2) experiment. As part of this experiment, almost daily ozonesonde launches were made between 17 April and 20 May 2002.

At the surface there is a strong diurnal variation with maximum ozone values in the afternoon (Figure 4.21). This results from strong losses at the site during the night when there is poor air ventilation from over the ocean and offshore flow often dominates. The afternoon ozone mixing ratios, however, generally represent well-ventilated flow that has an over-water fetch. There is a strong seasonal cycle in surface ozone (Figure 4.22) with an April maximum and a July minimum.

The intensive ozone profile measurements made during ITCT 2K2 were done during the seasonal maximum in tropospheric ozone (Figure 4.23). The cross-section of tropospheric ozone mixing ratio obtained from near daily ozonesondes during the ITCT 2K period (Figure 4.24) shows a series of large ozone mixing ratio events occurring every few days. These events often extend downward into the lower troposphere and occasionally extend to the surface. The boundary layer at the ozonesonde launching site is not usually well mixed with the layer above

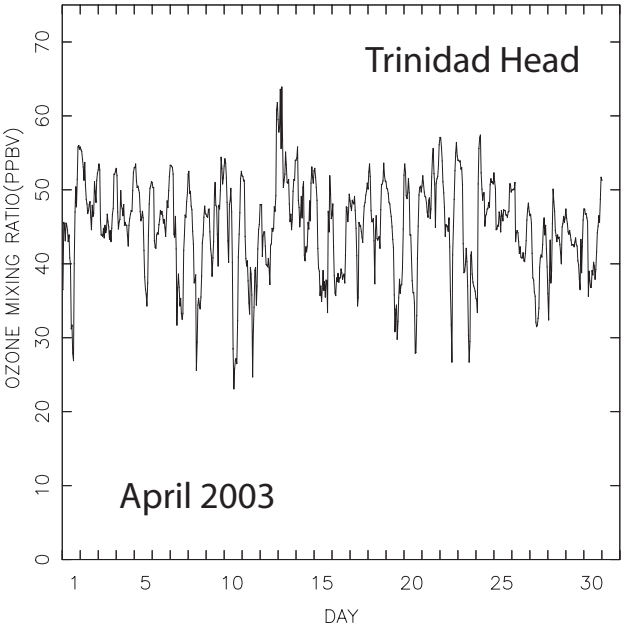

Figure 4.21. Hourly average ozone mixing ratios at Trinidad Head for April 2003. The values are plotted in Universal Time, which is 8 hours later than Pacific Standard Time (PST).

during the morning when the ozonesondes were launched. However, the afternoon average concentration at the Trinidad surface site has median values of 50 ppbv in April (Figure 4.22). In some of these strong enhancements it is possible to detect a stratospheric component in the layers below 5 km based on enhanced potential vorticity [*Cooper et al.*, 2004].

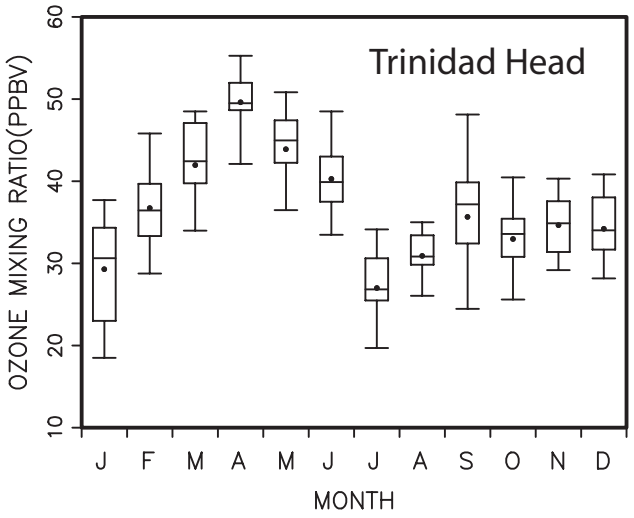

Figure 4.22. Monthly averages of the afternoon (1400–1800 PST) mean mixing ratio. The dot is the mean, the horizontal line inside the box is the median, the box is the inner 50th percentile, and the whiskers are the inner 90th percentile.

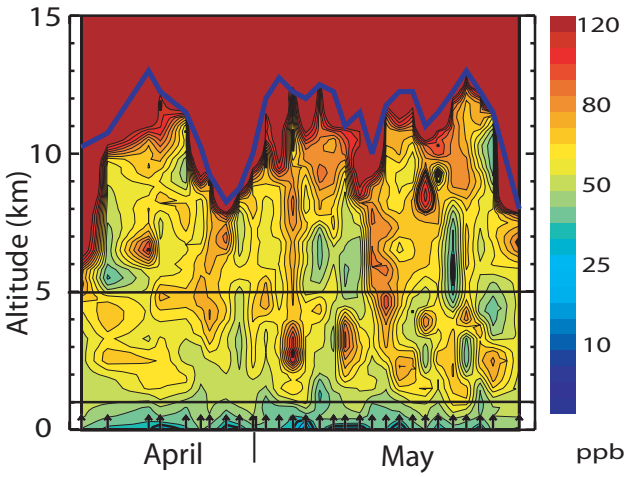

Figure 4.24. Cross-section of the tropospheric ozone mixing ratio during the spring of 2002 at Trinidad Head, California. The arrows at the bottom of the figure show the times when ozonesondes were launched. The solid blue line is the thermally defined tropopause. The solid horizontal lines at 1 km and 5 km represent the region where air mixed down from the upper troposphere and stratosphere is likely to remain in the lower troposphere.

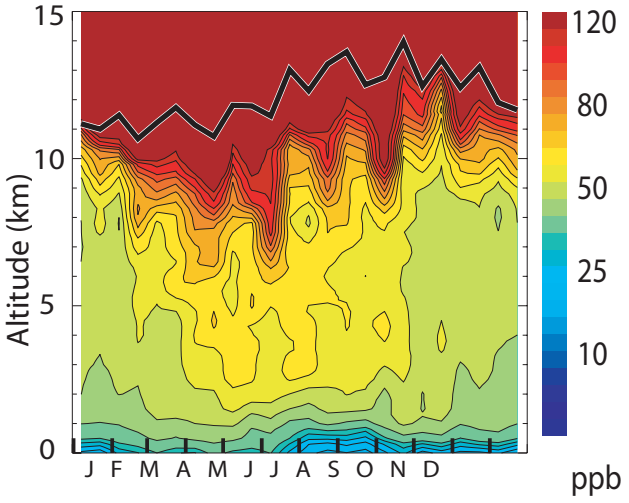

Figure 4.23. Seasonal cross-section of tropospheric ozone mixing ratio at Trinidad Head, California, based on 2-week averages from 280 ozone profile measurements from ozonesonde flights done between 1997–2003. The solid black line is the average tropopause height.

4.3. References

Antuña, J.C., A. Robock, G. Stenchikov, J. Zhou, C. David, J. Barnes, and L. Thomason (2003), Spatial and temporal variability of the stratospheric aerosol cloud produced by the 1991 Mount Pinatubo eruption, *J. Geophys. Res., 108*(D20), 4624, doi:10.1029/2003JD003722.

Antuña, J.C., A. Robock, G.L. Stenchikov, L.W. Thomason, and J.E. Barnes (2002), Lidar validation of SAGE II aerosol measurements after the 1991 Mount Pinatubo eruption, *J. Geophys. Res., 107*(D14), 4194, doi:10.1029/2001JD001441.

Barnes, J.E., S. Bronner, R. Beck, and N.C. Parikh (2003), Boundary layer scattering measurements with a CCD camera lidar, *Appl. Opt.*, *42*(15), 2647-2652.

Cooper, O., C. Forster, M. Trainer, D. Parrish, E. Dunlea, G. Hübler, F. Fehsenfeld, J. Holloway, S. Oltmans, B. Johnson, A. Wimmers, and L. Horowitz (2004), On the life cycle of a stratospheric intrusion and its subsequent large-scale mixing with warm conveyor belts, *J. Geophys. Res.*, *109*(D23S09), doi: 10.1029/2003JD00406.

Fetzer, E., L. McMillin, D. Tobin, H. Aumann, M. Gunson, W.W. McMillan, D. Hagan, M. Hofstadter, J. Yoe, D. Whiteman, J. Barnes, R. Bennartz, H. Vömel, V. Walden, M. Newchurch, P. Minnett, R. Atlas, F. Schmidlin, E. Olsen, M. Goldberg, S. Zhou, H. Ding, and H. Revercomb (2003), AIRS/AMSU/HSB validation, *IEEE Trans. Geosci. Remote Sens.*, *41*(2), 418-431.

Fujiwara, M., M. Shiotani, F. Hasebe, H. Vömel, S.J. Oltmans, P.W. Ruppert, T. Horinouchi, and T. Tsuda (2003), Performance of the Meteolabor "SnowWhite" chilled mirror hygrometer in the tropical troposphere: Comparisons with the Vaisala RS-80 A/H humicap sensors, *J. Atmos. Oceanic Technol, 20*(11), 1534-1542.

Harris, J.M., S.J. Oltmans, P.P. Tans, R.D. Evans, and D.L. Quincy (2001), A new method for describing long-term changes in total ozone, *Geophys. Res. Lett.*, *28*(24), 4535-4538, doi:10.1029/2001GL013501.

Johnson, B.J., S.J. Oltmans, H. Vömel, H.G.J. Smit, T. Deshler, and C. Kröger (2002), Electrochemical concentration cell (ECC) ozonesonde pump efficiency measurements and tests on the sensitivity to ozone of buffered and unbuffered-ECC sensor cathode solutions, *J Geophys. Res., 107*(D19), 4393, doi:10.1029/2001JD000557.

Mastenbrook, H.J., and J.E. Dinger (1960), The measurement of water vapor distribution in the stratosphere, *Tech. Rep. NRL 5551*, 35 pp., U.S. Naval Research Laboratory, Washington, D.C.

McPeters, R.D., G.J. Labow, and B.J. Johnson (1997), A satellite-derived ozone climatology for balloonsonde estimation of total column ozone, *J. Geophys. Res., 102*(D7), 8875-8885, doi:10.1029/96JD02977.

Müller, M., R. Neuber, F. Fierli, A. Hauchecorne, H. Vömel, and S.J. Oltmans (2003), Stratospheric water vapour as tracer for vortex filamentation in the Arctic winter 2002/2003, *Atmos. Chem. Phys., 3*(6), 1991-1997.

Oltmans, S.J., and D.J. Hofmann, Increase in lower-stratospheric water vapor at a midlatitude Northern Hemisphere site from 1981 to 1994 (1995), *Nature, 374*(6518), 146-149.

Ovarlez, J. (1989), H_2O measurements in the stratosphere and troposphere, *Procceedings of the 9th Symposium on European Rocket and Balloon Programs and Related Research*, pp. 299-303, European Space Agency, Lahnstein, FRG.

Press, W.H., S.A. Teukolsky, W.T Vetterling, and B.P. Flannery (1992), *Numerical Recipes in FORTRAN* (2nd ed.), 963 pp., Cambridge Univ. Press, New York.

Randel, W.J., F. Wu, S.J. Oltmans, K. Rosenlof, and G. Nedoluha (2004), Interannual changes of stratospheric water vapor and correlations with tropical tropopause temperatures, *J. Atmos. Sci*., in press.

Stark, P.A. (1970), *Introduction to Numerical Methods*, 334 pp., Macmillan, New York.

Vömel, H., S.J. Oltmans, D.J. Hofmann, T. Deshler, and J.M. Rosen (1995), The evolution of the dehydration in the Antarctic stratospheric vortex, *J. Geophys. Res., 100*(D7), 13,919-13,926, doi:10.1029/95JD01000.

Vömel, H., M. Rummukainen, R. Kivi, J. Karhu, T. Turunen, E. Kyrö, J.M. Rosen, N. Kjome, and S.J. Oltmans (1997), Dehydration and sedimentation of ice particles in the Arctic stratospheric vortex, *Geophys. Res. Lett., 24*(7), 795-798.

Vömel, H., S.J. Oltmans, B.J. Johnson, F. Hasebe, M. Shiotani, M. Fujiwara, N. Nishi, M. Agama, J. Cornejo, F. Paredes, and H. Enriquez (2002), Balloonborne observations of water vapor and ozone in the tropical upper troposphere and lower stratosphere, *J. Geophys. Res., 107*(D14), 10.1029/2001JD000707.

Vömel, H., M. Fujiwara, M. Shiotani, F. Hasebe, S. J. Oltmans, and J.E. Barnes (2003), The behavior of the Snow White chilled-mirror hygrometer in extremely dry conditions, *J. Atmos. Oceanic Tech., 20*(11), 1560-1567.